JACS
JOURNAL OF THE AMERICAN CHEMICAL SOCIETY
Communication
pubs.acs.org/JACS

Site-Specific Surface Functionalization of Gold Nanorods Using DNA Origami Clamps

Chenqi Shen,[†] Xiang Lan,[†] Xuxing Lu,[†] Travis A. Meyer,[‡] Weihai Ni,[†] Yonggang Ke,*[,‡] and Qiangbin Wang*[,†]

[†]Key Laboratory of Nano-Bio Interface, Division of Nanobiomedicine and *i*-Lab, Suzhou Institute of Nano-Tech and Nano-Bionics, Chinese Academy of Sciences, Suzhou 215123, China

[‡]Wallace H. Coulter Department of Biomedical Engineering, Georgia Tech and Emory University, Emory School of Medicine, Atlanta, Georgia 30322, United States

Supporting Information

ABSTRACT: Precise control over surface functionalities of nanomaterials offers great opportunities for fabricating complex functional nanoarchitectures but still remains challenging. In this work, we successfully developed a novel strategy to modify a gold nanorod (AuNR) with specific surface recognition sites using a DNA origami clamp. AuNRs were encapsulated by the DNA origami through hybridization of single-stranded DNA on the AuNRs and complementary capture strands inside the clamp. Another set of capture strands on the outside of the clamp create the specific recognition sites on the AuNR surface. By means of this strategy, AuNRs were site-specifically modified with gold nanoparticles at the top, middle, and bottom of the surface, respectively, to construct a series of well-defined heterostructures with controlled "chemical valence". Our study greatly expands the utility of DNA origami as a tool for building complex nanoarchitectures and represents a new approach for precise tailoring of nanomaterial surfaces.

Surface functionalities of nanomaterials play a particularly decisive role in regulating their physical and chemical properties, such as biocompatibility[1] and catalytic activity,[2] because of their high surface-to-volume ratios. Therefore, methods for surface modification of nanoparticles have been investigated in depth. Classic surface modification processes isotropically decorate the whole nanoparticle surface, thus creating a single type of surface functionality.[3] In recent years, more efforts have been dedicated to fabricating surface-anisotropic nanoparticles displaying multiple surface functionalities[4] by utilizing methods such as deposition,[5] lithography,[6] templating,[7] etc. Nonetheless, these anisotropic functionalization methods still lack the precision needed to manufacture functional nanomaterials with custom-designed individual recognition sites. A new strategy that can generate nanomaterial surfaces with arbitrary single-site modifications could facilitate the construction of new nanomaterials with greater complexity and potentially new functionalities.

DNA has emerged as a powerful molecule for surface-anisotropic functionalization[8] because of its outstanding features including sequence programmability,[9] distinctive molecular recognition,[10] and facile chemical modifications.[11] For instance, Mirkin and co-workers[12] fabricated gold nanoparticles (AuNPs) asymmetrically surface-functionalized with both normal and extended oligonucleotides with the assistance of magnetic microparticles, and these anisotropic particles were further used as building blocks for the construction of unique heterostructures. With the advancement of DNA nanotechnology, self-assembled DNA origami has proven to be a versatile platform for constructing fully addressable, arbitrary-shaped nanostructures.[13] Noble-metal nanoparticles,[14] quantum dots,[15] fluorescent probes,[16] and biomolecules[17] have been precisely docked to specific locations on DNA origami scaffolds to fabricate a variety of well-ordered nanoarchitectures. Therefore, the use of DNA origami could be a promising technique to realize single-site surface modification of nanoparticles, which has not been reported before.

In this work, we developed a novel strategy to render a gold nanorod (AuNR) with specific surface recognition sites using a DNA origami nanostructure. An open DNA origami nanostructure, termed a "DNA clamp", was designed with capture strands on the inside faces, causing the DNA clamp to close around the AuNR after hybridization with the complementary DNA strands on the AuNR surface, fully encapsulating the nanorod surface. The DNA-clamp-covered AuNR possesses a fully addressable surface, offering unprecedented site-specific functionality and promising more precise construction of complex nanostructures. Furthermore, this new approach expands the usage of DNA origami from addressable assembly of functional components to site-specific surface modification of nanomaterials, enabling the rational design and precise fabrication of functional nanomaterials and nanostructures.

Figure 1 schematically illustrates the step-by-step process for surface functionalization of the AuNR. First, a DNA clamp consisting of two half-tubes with equal lengths of 56 nm linked by two flexible hinges was designed. A total of 16 capture strands were arranged in three stripes protruding from the inside faces of the DNA clamp. A 13 nm × 38 nm AuNR functionalized with thiolated single-stranded DNA (ssDNA) was mixed with the self-assembled DNA clamp, leading to hybridization of ssDNA on the AuNR surface with the complementary capture strands inside the clamp. This

Received: November 4, 2015
Published: January 29, 2016

DOI: 10.1021/jacs.5b11566
J. Am. Chem. Soc. 2016, 138, 1764−1767

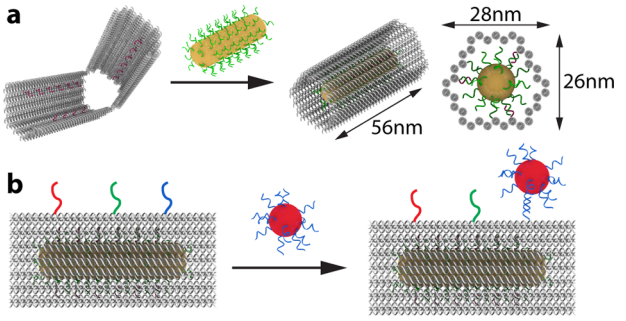

Figure 1. Scheme showing the process for surface functionalization of a AuNR. (a) The AuNR was first modified with thiolated ssDNA. The ssDNA-functionalized AuNR was then encapsulated by the DNA clamp (with a size of 26 nm × 28 nm in solution) through hybridization with the capture strands inside the clamp. (b) Three groups of capture strands outside the clamp formed three specific recognition sites on the AuNR surface after functionalization by the DNA clamp. A collection of heteroassemblies was then created with the addition of AuNPs modified with different complementary ssDNA to test the site selectivity of the AuNR.

hybridization drives the DNA clamp to close and encapsulate the AuNR, forming a hexagonal cross section with a maximum length and width of 28 and 26 nm (Figure 1a). To demonstrate the site selectivity of the DNA-clamp-modified AuNR, we introduced three groups of unique capture strands protruding from the outer surface of the DNA clamp, as shown in Figure 1b. The functionalized AuNR thus possessed three specific recognition sites, located at the top, middle, and bottom of the AuNR surface. We then added AuNPs functionalized with corresponding complementary DNA sequences to build a series of AuNR−AuNP heteroassemblies with precise spatial configurations.

The ssDNA-modified AuNRs, DNA-clamp-covered AuNRs, and AuNR−AuNP heteroassemblies were subsequently analyzed by agarose gel electrophoresis. The resulting gel images under daylight and UV light are shown in Figure 2a,b, respectively. Lane 1 corresponds to the ssDNA-modified AuNRs, while lane 2 contains AuNRs covered by the DNA clamp. The decreased mobility of the target band in lane 2 is presumably due to the extra resistance added by the DNA clamp. Lanes 3−5 represent the site-selective AuNRs assembled with one (top site), two (top and bottom sites), and three (top, middle, and bottom sites) 6 nm-sized AuNPs, respectively. A slight decrease in the mobility of each assembly was observed with successive additions of AuNPs. Lane 6 corresponds to the DNA clamp as a reference, which possessed similar mobility as the DNA-clamp-covered AuNR.

The self-assembled DNA clamp and the site-selective DNA-clamp-covered AuNRs were confirmed by transmission electron microscopy (TEM) after purification, as shown in Figure 2c,d. The negative-stained two-dimensional TEM images of the open DNA clamp showed that it possessed two half-tubes connected by flexible hinges. Each half-tube exhibited a quasi-rectangular morphology matching our design. The length of each half-tube was approximately 50 nm, which is consistent with our design and similar to the length of the AuNRs. Hybridization between the ssDNA on the AuNR surface and the complementary capture strands inside the DNA clamp led to a final core−shell nanoarchitecture with the DNA clamp covering the AuNR with a thickness of 2 nm in the dried state. Because of its lower contrast in TEM measurements, the DNA clamp around the

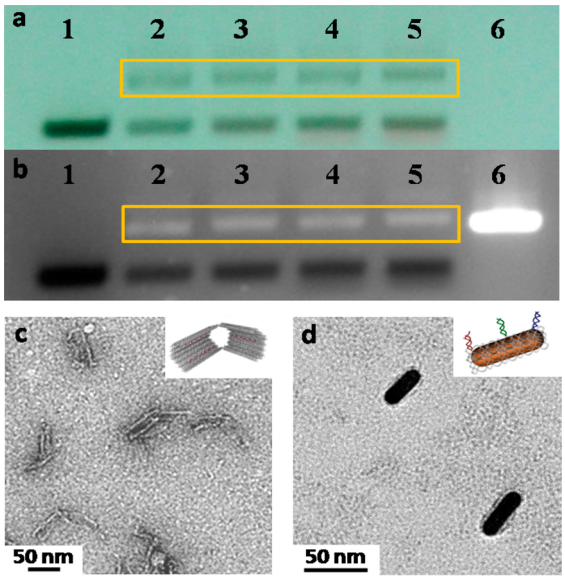

Figure 2. Characterization of the DNA clamp and the functionalized AuNRs. (a) Daylight- and (b) UV-light-illuminated agarose gel images of the AuNRs and their heteroassemblies with AuNPs. Lane 1: ssDNA-modified AuNRs. Lane 2: site-selective DNA-clamp-covered AuNRs. Lanes 3−5: AuNR−AuNP heteroassemblies containing one (top site), two (top and bottom sites), or three (top, middle, and bottom sites) 6 nm AuNPs. Lane 6: the DNA origami clamp. The target products in lanes 2−5 are highlighted by the yellow boxes. (c, d) Negative-stained TEM images of (c) DNA clamps and (d) site-selective AuNRs.

AuNR was a halo, the thickness of which was visible as ∼2 nm in the TEM images (Figure 3a).

To verify our strategy for site-specific functionalization of the AuNRs, AuNPs conjugated with ssDNA sequences complementary to the three groups of capture strands on the outer surface of the DNA clamp were added to construct a set of well-defined AuNR−AuNP heterostructures. It should be noted that because of the flexibility of the DNA double helix, the position of the AuNPs docked on the AuNR surface might shift under TEM measurement. Taking this point into account, we predicted that the maximum distance from the site-specifically docked AuNPs to the DNA clamp covering the AuNR surface would be 7.5 nm (Figure 3a), considering that the capture strands on the outer surface of the DNA clamp were 22 base pairs long. Therefore, all of the samples with distances between the AuNP and DNA clamp smaller than 7.5 nm were considered the products that were hybridized through our site-specific functionalization strategy.

At first, a single AuNP was introduced at either top or middle site of the AuNR to verify the site-selective functionalization strategy. As presented in Figure 3b,c, the TEM images clearly illustrate that most of the AuNRs had a 6 nm-sized AuNP selectively attached at the top or middle site, respectively. The statistical analysis indicated that up to 84% or 90% of the products, respectively, possessed distances from the AuNP to the DNA clamp shorter than 7.5 nm, which verifies the high efficiency of our strategy in precisely constructing AuNRs with site-selective functionality. The small population with distances longer than 7.5 nm was possibly attributable to incomplete hybridization of the AuNP and the DNA clamp on the AuNR surface or loose encapsulation of the AuNR by the DNA clamp. In another set of experiments, a larger 8.5 nm-sized AuNP was

DOI: 10.1021/jacs.5b11566
J. Am. Chem. Soc. 2016, 138, 1764−1767

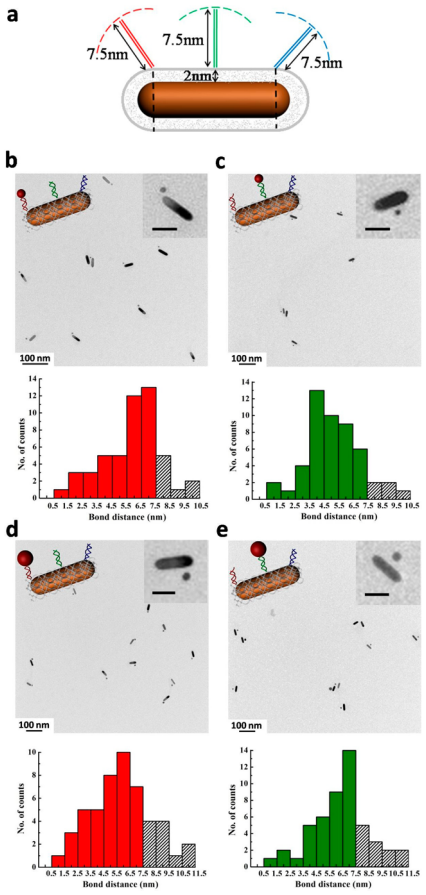

Figure 3. Site-specific functionalization of AuNRs with a single AuNP. (a) Schematic model of the maximum distance between the AuNP and the DNA clamp. (b, c) TEM images and distance distributions of a 6 nm-sized AuNP site-selectively anchored (b) at the top (red) or (c) at the middle (green) of a AuNR. (d, e) TEM images and distance distributions of an 8.5 nm-sized AuNP site-selectively anchored (d) at the top (red) or (e) at the middle (green) of a AuNR. The colored columns in the histograms represent the populations of the formed AuNR–AuNP heterostructures with distances shorter than 7.5 nm, while the dashed columns represent the populations of the dislocated assemblies with distances larger than 7.5 nm. The scale bars in zoomed-in TEM images (insets) are 25 nm.

selectively assembled on the AuNR surface. Similar to experiments with the 6 nm-sized AuNPs, we observed that most of the AuNPs were located at the top (78%) or middle (76%) site of the AuNR at a distance between the AuNP and the DNA clamp shorter than 7.5 nm, as shown in Figure 3d,e. This slightly decreased yield was attributed to steric hindrance due to the increased size of the AuNPs.

Next, the proposed site-selective functionalization strategy was further proved by introducing two AuNPs at specific sites of a AuNR to assemble complex nanostructures. Figure 4 exhibits a collection of TEM images and distance distributions of these assemblies following hybridization of 6 nm- and 8.5 nm-sized AuNPs at two of the three sites of a AuNR. The TEM images show that the two different-sized AuNPs were site-specifically located on the AuNR surface through the hybridization of ssDNA on the AuNPs.

Finally, three AuNPs were hybridized with the DNA clamp to achieve more complex AuNR–AuNP heterostructures in which the localization of the AuNPs on the AuNR surface was precisely controlled by the site selectivity of the DNA clamp.

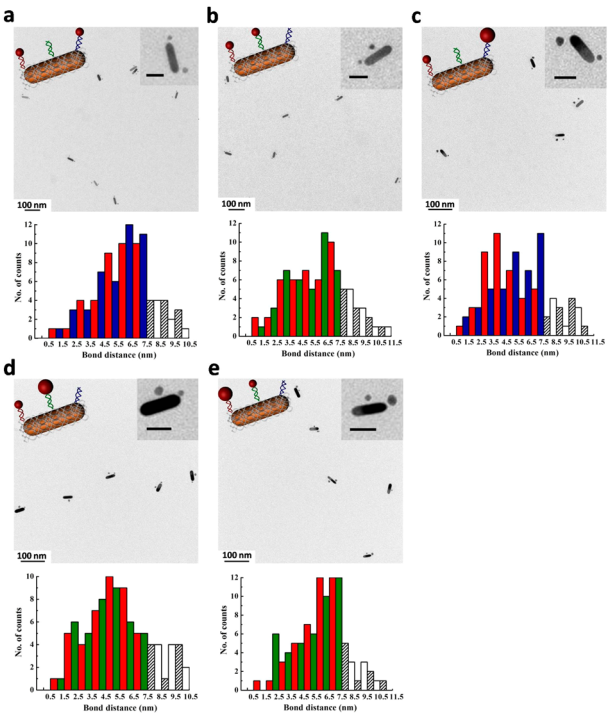

Figure 4. TEM images and distance distributions of the assemblies of AuNRs with two AuNPs: (a) two 6 nm-sized AuNPs at the top and bottom sites of the AuNR; (b) two 6 nm-sized AuNPs at the top and middle sites of the AuNR; (c) one 6 nm-sized AuNP and one 8.5 nm-sized AuNP at the top and bottom sites of the AuNR; (d) one 6 nm-sized AuNP at the top site and one 8.5 nm-sized AuNP at the middle site of the AuNR; (e) one 8.5 nm-sized AuNP at the top site and one 6 nm-sized AuNP at the middle site of the AuNR. Red, green, and blue colors represent bonds formed at the top, middle, and bottom sites, respectively. The scale bars in the zoomed-in TEM images (insets) are 25 nm.

The TEM images in Figure 5 show that the AuNPs were docked at the top, middle, and bottom sites of the AuNR, fully confirming the precise site selectivity of the AuNR surface.

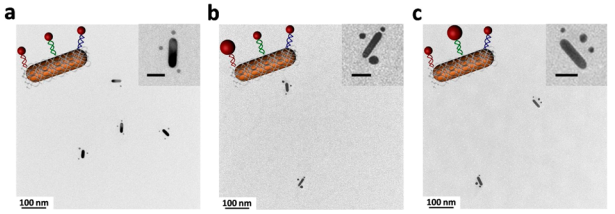

Figure 5. TEM images of assemblies of AuNRs with three AuNPs: (a) three 6 nm-sized AuNPs at the top, middle, and bottom sites of the AuNR; (b) one 8.5 nm-sized AuNP at the top site and two 6 nm-sized AuNPs at the middle and bottom sites of the AuNR; (c) one 8.5 nm-sized AuNP at the middle site and two 6 nm-sized AuNPs at the top and bottom sites of the AuNR. The scale bars in the zoomed-in TEM images (insets) are 25 nm.

In summary, we have successfully demonstrated precise control of the AuNR's surface functionality, including modulation of its chemical valence from monovalent to divalent and trivalent as well as the site-specific functionality from the top to the middle and bottom of the AuNR, by taking advantage of DNA nanotechnology. A DNA clamp was employed to encapsulate the AuNR and form the AuNR@

DOI: 10.1021/jacs.5b11566
J. Am. Chem. Soc. 2016, 138, 1764–1767

DNA clamp core@shell structure, in which the DNA clamp endowed the AuNR with controlled chemical valence and site-specific functionality after rational design of the sequence and location of the capture strands protruding from the DNA clamp. AuNPs conjugated with DNA sequences complementary to the protruding sequence on the DNA clamp were hybridized with the AuNR, and different patterns of AuNR–AuNP heterostructures were assembled in high yield, demonstrating the success of our site-selective AuNR functionalization strategy. Our strategy represents a new approach for precisely tailoring the nanoparticle surface, and we expect to realize site-specific tuning of significant optical properties such as surface-enhanced Raman spectroscopy and metal-enhanced fluorescence from these precisely controlled nanoarchitectures. Additionally, site-selective catalysis might be achieved, and a smart cascade catalytic reaction system could be further designed since we can precisely control the spatial location of the catalytic sites.

■ ASSOCIATED CONTENT

Supporting Information

The Supporting Information is available free of charge on the ACS Publications website at DOI: 10.1021/jacs.5b11566.

Experimental details, more TEM images, UV–vis extinction spectra, electromagnetic field simulations, schematic description of the DNA clamp, and DNA sequences (PDF)

■ AUTHOR INFORMATION

Corresponding Authors

*yonggang.ke@emory.edu

*qbwang2008@sinano.ac.cn

Notes

The authors declare no competing financial interest.

■ ACKNOWLEDGMENTS

This work was supported by grants from the Chinese Academy of Sciences "Strategic Priority Research Program" (XDA01030200) and the National Natural Science Foundation of China (21425103) to Q.W. and a grant from the Biomedical Engineering Department Startup Fund and a Billi and Bernie Marcus Research Award to Y.K. T.A.M. was supported by an NSF Graduate Research Fellowship (Grant DGE-1148903).

■ REFERENCES

(1) Mout, R.; Moyano, D. F.; Rana, S.; Rotello, V. M. *Chem. Soc. Rev.* **2012**, *41*, 2539.

(2) (a) Niu, Z.; Li, Y. *Chem. Mater.* **2014**, *26*, 72. (b) Mahmoud, M. A.; Narayanan, R.; El-Sayed, M. A. *Acc. Chem. Res.* **2013**, *46*, 1795.

(3) (a) Bagwe, R. P.; Hilliard, L. R.; Tan, W. *Langmuir* **2006**, *22*, 4357. (b) Rieter, W. J.; Taylor, K. M. L.; Lin, W. *J. Am. Chem. Soc.* **2007**, *129*, 9852. (c) Bilan, R.; Fleury, F.; Nabiev, I.; Sukhanova, A. *Bioconjugate Chem.* **2015**, *26*, 609.

(4) (a) Glotzer, S. C.; Solomon, M. J. *Nat. Mater.* **2007**, *6*, 557. (b) Pradhan, S.; Xu, L.; Chen, S. *Adv. Funct. Mater.* **2007**, *17*, 2385. (c) Song, Y.; Liu, K.; Chen, S. *Langmuir* **2012**, *28*, 17143.

(5) Pawar, A. B.; Kretzschmar, I. *Langmuir* **2009**, *25*, 9057.

(6) Zhang, G.; Wang, D.; Möhwald, H. *Nano Lett.* **2005**, *5*, 143.

(7) Jones, M. R.; Osberg, K. D.; Macfarlane, R. J.; Langille, M. R.; Mirkin, C. A. *Chem. Rev.* **2011**, *111*, 3736.

(8) (a) Tan, L. H.; Xing, H.; Chen, H.; Lu, Y. *J. Am. Chem. Soc.* **2013**, *135*, 17675. (b) Millstone, J. E.; Georganopoulou, D. G.; Xu, X.; Wei, W.; Li, S.; Mirkin, C. A. *Small* **2008**, *4*, 2176. (c) Liu, W.; Liu, D.; Zhu, Z.; Han, B.; Gao, Y.; Tang, Z. *Nanoscale* **2014**, *6*, 4498. (d) Xu, L.; Kuang, H.; Xu, C.; Ma, W.; Wang, L.; Kotov, N. A. *J. Am. Chem. Soc.* **2012**, *134*, 1699. (e) Jones, M. R.; Seeman, N. C.; Mirkin, C. A. *Science* **2015**, *347*, 1260901.

(9) Song, T.; Tang, L.; Tan, L. H.; Wang, X.; Satyavolu, N. S. R.; Xing, H.; Wang, Z.; Li, J.; Liang, H.; Lu, Y. *Angew. Chem., Int. Ed.* **2015**, *54*, 8114.

(10) Wang, Q.; Yang, X.; Wang, K.; Tan, W.; Gou, J. *Analyst* **2008**, *133*, 1274.

(11) Hardisty, R. E.; Kawasaki, F.; Sahakyan, A. B.; Balasubramanian, S. *J. Am. Chem. Soc.* **2015**, *137*, 9270.

(12) Xu, X.; Rosi, N. L.; Wang, Y.; Huo, F.; Mirkin, C. A. *J. Am. Chem. Soc.* **2006**, *128*, 9286.

(13) (a) Iinuma, R.; Ke, Y.; Jungmann, R.; Schlichthaerle, T.; Woehrstein, J. B.; Yin, P. *Science* **2014**, *344*, 65. (b) Wang, R.; Nuckolls, C.; Wind, S. J. *Angew. Chem., Int. Ed.* **2012**, *51*, 11325. (c) Yao, G.; Li, J.; Chao, J.; Pei, H.; Liu, H.; Zhao, Y.; Shi, J.; Huang, Q.; Wang, L.; Huang, W.; Fan, C. *Angew. Chem., Int. Ed.* **2015**, *54*, 2966. (d) Zhou, C.; Duan, X.; Liu, N. *Nat. Commun.* **2015**, *6*, 8102.

(14) (a) Kuzyk, A.; Schreiber, R.; Fan, Z.; Pardatscher, G.; Roller, E.-M.; Högele, A.; Simmel, F. C.; Govorov, A. O.; Liedl, T. *Nature* **2012**, *483*, 311. (b) Chen, Z.; Lan, X.; Wang, Q. *Small* **2013**, *9*, 3567. (c) Li, Y.; Liu, Z.; Yu, G.; Jiang, W.; Mao, C. *J. Am. Chem. Soc.* **2015**, *137*, 4320. (d) Tian, Y.; Wang, T.; Liu, W.; Xin, H. L.; Li, H.; Ke, Y.; Shih, W. M.; Gang, O. *Nat. Nanotechnol.* **2015**, *10*, 637.

(15) (a) Schreiber, R.; Do, J.; Roller, E.; Zhang, T.; Schüller, V. J.; Nickels, P. C.; Feldmann, J.; Liedl, T. *Nat. Nanotechnol.* **2014**, *9*, 74. (b) Samanta, A.; Deng, Z.; Liu, Y. *Nanoscale* **2014**, *6*, 4486.

(16) Pal, S.; Dutta, P.; Wang, H.; Deng, Z.; Zou, S.; Yan, H.; Liu, Y. *J. Phys. Chem. C* **2013**, *117*, 12735.

(17) Jusuk, I.; Vietz, C.; Raab, M.; Dammeyer, T.; Tinnefeld, P. *Sci. Rep.* **2015**, *5*, 14075.

DOI: 10.1021/jacs.5b11566
J. Am. Chem. Soc. 2016, 138, 1764–1767